Vol. 18, No. 1 (2019) 13-26
Revista Mexicana de Ingeniería Química

CREVICES CORROSION IN CRACKS OF AISI-410 USED IN STEAM TURBINES BLADES

CORROSIÓN POR HENDIDURA EN GRIETAS DEL AISI-410 USADO EN ALABES DE TURBINAS DE VAPOR

C. Cuevas-Arteaga*, C.M. Clemente, J.A. Rodríguez
Centro de Investigación en Ingeniería y Ciencias Aplicadas, Universidad Autónoma del Estado de Morelos. Av. Universidad 1001, Col. Chamilpa, CP-62209, Cuernavaca, Mor., México.
Received April 16, 2018; Accepted june 12, 2018

Abstract

In this paper the effect of temperature on corrosion crack propagation produced in a stainless steel AISI-410 type was studied. The previously cracked specimens through a rotatory machine were exposed in seawater during 5 days at two temperatures (25 °C and 90 °C). The corrosion process was studied using the electrochemical noise technique (EN) and potentiodynamic polarization curves (PC). The electrochemical noise time series were used to analyze the changes in corrosion activity for AISI-410 under the mentioned experimental conditions determining the type and corrosion rate. The results show that cracks will grow when are exposed to seawater, especially at high temperatures. Physical characterization obtained from SEM reveals a great amount of corrosion products emerging from the cracks as evidence of the oxidation of the material, causing a mixed corrosion type around the cracks: uniform and pitting. From the results, it is concluded that the corrosion attack in the cracks may influence crevice corrosion, which eventually leads to stress corrosion cracking and corrosion fatigue.
Keywords: Corrosion, electrochemical noise, cracks, pitting, AISI-410.

Resumen

En este artículo los efectos de la temperatura sobre la propagación de la corrosión en grietas producidas en el acero inoxidable 410 fueron estudiados. Especímenes previamente agrietados usando una máquina rotatoria fueron expuestos en agua de mar durante 5 días a dos temperaturas (25 ºC y 90 ºC). La corrosión fue estudiada usando las técnicas electroquímicas de ruido y curvas de polarización potenciodinámicas. Las series de tiempo del ruido electroquímico fueron usadas para analizar los cambios en la actividad corrosiva del AISI-410 determinando el tipo y la velocidad de corrosión. Los resultados mostraron que las grietas crecieron al ser expuestas en agua de mar, especialmente a altas temperaturas. La caracterización física obtenida mediante microscopia electrónica de barrido presentó una gran cantidad de productos de corrosión emergiendo de las grietas como evidencia de la oxidación del material, causando un tipo de corrosión mixto alrededor de las grietas: uniforme y picaduras. De esta investigación pudo deducirse que el ataque corrosivo in las grietas puede influenciar la corrosión por hendidura, la cual eventualmente encamina a la corrosión bajo tensión y a la corrosión por fatiga.
Palabras clave: Corrosión, ruido electroquímico, grietas, picaduras, AISI-410.

1 Introduction

Many authors have studied the behavior of pitting process in components or mechanical parts present in seashore, petroleum platforms, steam turbines blades, oil and gas pipelines, bridges, marine and planes structures, vessels containing corroding fluids or gases, etc. (Kuviak *et al*., 2005). The accumulation of damage due to localized corrosion, pitting, stress corrosion cracking and corrosion fatigue in low pressure steam turbines components, such as blades, discs and rotors has been consistently identified as the main causes of turbine failure among others. In recent years, significant efforts have been devoted

* *Corresponding author. E-mail*: ccuevas@uaem.mx
Tel. 777 3297084, Fax 777 3 297984.
doi: https://doi.org/10.24275/uam/izt/dcbi/revmexingquim/2019v18n1/Cuevas
issn-e: 2395-8472

to developing non-destructive techniques for damage identification with respect to failures of blades in steam turbines, which represents a serious loss of availability and reliability.

Kubiak *et al*. (2005) found that the blades of the last stage known as "L-0 stage" and localized in the low pressure zone of a steam turbine of 37.5 MW were exposed to corrosion by sulfates and erosion by moisture, which reduced the useful life to 120,000-140,000 hours, being the average useful life of a steam turbine of 350,400 hours. In the last stages of condensing steam turbines low pressures and temperatures near of 90 ºC the sulfates are present and the phase changes could occur easily. On the other hand the blades are larger than in other stages, which lead to high stress due to centrifugal forces and steam forces. Also if there are dynamic forces due to vibrations, this could increase such stress. The blades of the last stage of steam turbines are subject to corrosive environment and cyclic load, which could lead to failures due to crack propagation and corrosion. Such blades with different mechanisms of corrosion such as localized corrosion, pitting, stress corrosion cracking and corrosion fatigue are frequently observed. It is believed that this corrosion phenomenon is mainly presented due to the transportation of impurities from the condensate fluid and from the steam together with the high concentration of dirt in liquid films on the blade and disc surfaces, which during shutdown conditions lead to localized corrosion and pitting. Therefore the steam turbine blades are simultaneously exposed to cyclic load and corrosive environments at elevated temperatures. Crack initiation is present when a small area is depassivated becoming an anodic area, while the area around the anodic area becomes cathodic zones leading to localized galvanic corrosion. Usually a lack of oxygen in the crack could promote crack propagation (Turnbull *et al*., 2011). Some corrosion reports from corroded steam turbine blades have indicated the presence of sulfur, chlorine, sodium and oxygen together with the main elements forming the alloy (used to design and build the blades) are present in the corrosion products. The presence of oxygen evidences the formation of metallic oxides, since the metallic elements tend to go back to their original condition in nature becoming oxides, which presumably protect the surface forming a passive layer. The passive layer can be broken or dissolved leaving the material susceptible to corrosion when exposed to an aggressive environment. The presence of sulfur and chlorine indicates the probably formation of secondary compounds such as metallic chlorines and metallic sulfides. Sulfur together with sodium may lead to metallic sulfates. Also the presence of these complex compounds shows that the initially formed metallic oxides are dissolved, so the alloy is not protected anymore and the corrosion rate would be very high. The type of attack can be of different ways, including pitting as localized corrosion or even internal corrosion such as intergranular sulfidation, which inclusively lead to catastrophic corrosion resulting in a shutdown condition. So that, in order to understand the corrosion mechanism of localized corrosion as pitting corrosion or crevice corrosion in steam turbines blades it is important to study these possible processes in order to confirm the corrosion attack and the corrosion rate of AISI-410 and the influence of an increment of temperature.

Electrochemical techniques are tools for evaluating the corrosion rate and the type of corrosion that metals or alloys suffer when they are immersed in an electrolyte at different temperatures and under different loads (Baboian, 2002). One of such methods is the electrochemical noise (EN) in potential and current. Through this technique, the corrosion activity is monitored measuring the current or potential as function of exposure time (Andrade *et al*. 2010). Noise signals in current and potential can display low frequency of high intensity transient, which indicates rupture of the passive layer formed by metallic oxides and pitting nucleation as a type of localized corrosion (Sánchez *et al*., 2009). The presence of cracks and its possible modifications by corrosion can also be studied by EN. EN results can be analyzed using statistical procedures by determining some parameters such as the arithmetic mean, median and standard deviation in the time domain and localized index (Tristancho *et al*., 2004; Cuevas, 2006; Cuevas 2008). Localized index together with the physical evidences can help to determine the type of corrosion suffered by the studied materials.

In this paper the effect of temperature and corrosive environment on the crack growth in samples of AISI-410 was studied. The cracks were previously achieved through a mechanical fatigue process according to the standard ASTM E 647-88A (2011) using a rotary cylinder machine for testing fatigue at a frequency of 28 Hz. The cracked samples were immersed in natural sea water during 5 days at 25 ºC and 90 ºC. The corrosion parameters were determined using the electrochemical noise technique and potentiodynamic polarization curves. The main contribution of this work was to determine the

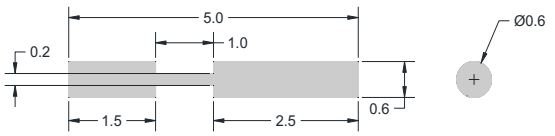

Fig. 1. Specimen dimensions of AISI-410 exposed to sea water at 25 and 90 ºC.

corrosion rate and the corrosion mechanism of AISI-410 stainless steel in presence of cracks and the way in which such previously induced cracks may influence pitting and crevice corrosion in time.

2 Materials and methods

The studied material was the stainless steel AISI-410 used as a standard material for steam turbine blades of the last stage at low pressure. Several specimens with the following dimensions as shown in Fig. 1 were exposed to seawater at two temperatures (25 ºC and 90 ºC).

Before the exposure to fatigue the specimens were cut from the same material AISI-410. Then the specimens were subjected to fatigue according to ASTM E 647-88A (2011) using a rotary cylinder machine for testing fatigue Moore model RBF-200 (See diagram of Fig. 2). Table 1 shows the frequency values and the load to which the specimens were subjected to fatigue testing, whose results are expressed in terms of the number of cycles and the cracks size (Cuevas *et al*., 2013). This technique involves fatigue cycles through which the crack occurs. The crack length was measured by means of a Scanning Electron Microscopy (SEM) before being exposed to the corrosive environment as shown in Fig. 3a and 3b. The sample presented in Fig. 3a was used for the experiment at room temperature (25 ºC) whereas the sample presented in Fig. 3b was used for the experiment at 90 ºC.

Sample A presented a crack of 3160 μm long and 7.95 μm width corresponding to 5.0382×10^4 cycles; whereas sample B presented a crack of 2320.8 μm long and 8.57 μm width corresponding to 6.0216×10^4 cycles. The specimens with the cracks such as explained in the above paragraph were used for making the working electrodes for the electrochemical cells when applying the current and potential noise technique and the potentiodynamic polarization curves.

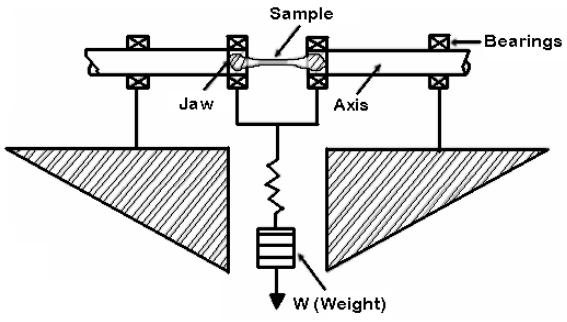

Fig. 2. Diagram of the rotary cylinder machine for testing fatigue.

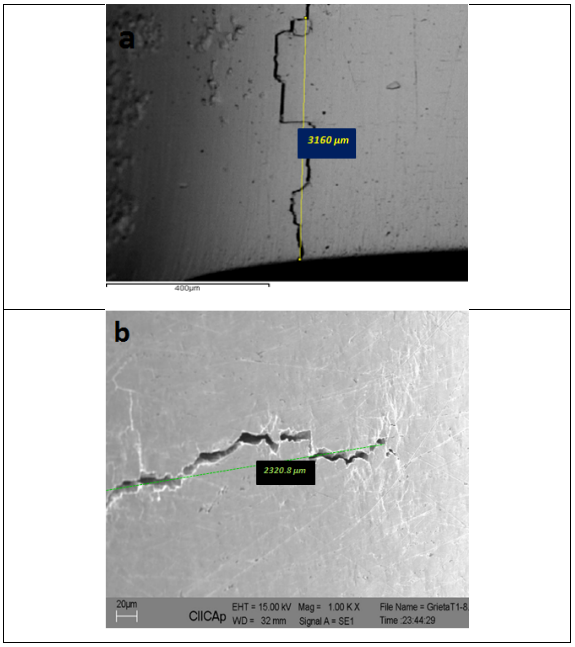

Fig. 3. a) Micrograph of the specimen A with a crack length of 3160 μm and a width of 7.95 μm. b) Micrograph of the specimen B with a crack length of 2320.8 μm and a width of 8.57 μm.

One specimen was analyzed by EDX obtaining its chemical composition (See Table 2). It is possible to anticipate that the presence of chromium can be a helpful factor to improve the corrosion resistance of this material, nevertheless the great amount of iron can make it susceptible to suffer localized corrosion since its oxides are easily dissolved becoming porous and non-adherent.

Table 1. Frequency values and loading cycles of samples A and B used in corrosion tests at 25 and 90 ºC.

Sample	Frequency	N (Cycles)	Load (MPa)
A	28	5.0382×10^4	0.1310
B	28	6.0216×10^4	0.1241

Table 2. Chemical composition of AISI 410 stainless steel before exposure to corrosion.

Element	Weight %
Iron	80.108
Chromium	14.014
Silicon	1.212
manganese	1.131
molybdenum	0.589
nickel	0.403
carbon	2.543

Specimens used as electrodes in the electrochemical cells were metallographically prepared according to the standard ASTM G1-03 (2017) before exposing to corrosion and EDX analysis. Then the samples A and B were cleaned according to standard ASTM G31-72 (2004) utilizing distilled water and acetone and eventually dried with hot air. To get an electrical connection between the electrodes and electrochemical measuring equipment each specimen was welded to a wire of nicromel (80% wt. Ni-20% wt. Cr) 1mm in diameter and 150 mm long. The conductor wire was insulated by inserting it into a glass tube of 5 mm inner diameter. The space between the conductor wire and the walls of the glass tube was sealed with an epoxy resin. The tests were conducted at two temperatures 25 ºC and 90 ºC. The next step was to set up the electrochemical cells for the EN technique composed of three electrodes of the same material in accordance with the ASTM G199-09 (2014), two of them in the form of rectangular parallelepipeds with no cracks and the third one presenting the crack as shown in Figure 4a. The corrosive medium was 250 ml of natural seawater contained in a flask. The cracked specimen A was exposed to 25 ºC whereas the cracked specimen B was exposed to 90 ºC accordingly to Table 3. Polarization curves were obtained using an electrochemical cell constituted by a working electrode (AISI-410 sample with crack) a reference electrode and an auxiliary electrode both prepared of platinum wires. Polarization curves were obtained by applying an over-potential from −200 mV to 1500 mV with a scan rate of 1 mV/s.

Table 3. Nomenclature of the specimens.

Cracked Specimen	Temperature
A	25° C
B	90° C

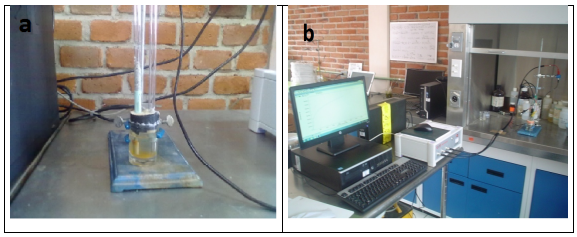

Fig. 4. Photographs of the experimental set up of the electrochemical tests.

Table 4. Chemical composition of natural seawater.

Element	ppm (100ml)	Element	ppm (100 ml)
Cr	0.91	Fe	0.57
Cu	0.074	K	400.0
Ni	0.74	Na	9361.0
Pb	0.62	Ca	645.0
Zn	0.20	Mg	1420.0
Cd	0.16	Sulfates	7390.0
Mn	0.069	Chlorides	20940.0

For both electrochemical measurements an ACM Instruments potentiostat/galvanostat model 1120 was used (Figure 4b). In order to determine the composition of the natural sea water as the corrosive medium, 100 ml of the solution were analyzed trough the atomic absorption technique which results are presented in Table 4 in parts per million. The pH of the solution was measured as 8. The presence of high content of sulfates and especially of chlorides makes the corrosive solution very aggressive especially for stainless steel, which is susceptible to suffer localized corrosion. After exposing the sample A at 25 ºC and sample B at 90 ºC during five days applying the EN technique both samples with and without corrosion products were analyzed by SEM. In order to determine the type of corrosion products generated during the corrosion process, EDX analyses were also made to the corrosion products covering the metallic surface after the immersion.

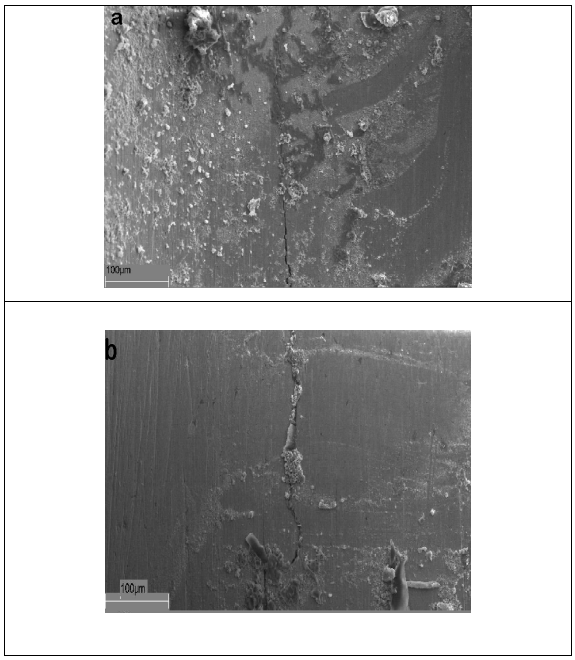

Fig. 5. Micrographs of sample A after exposure at 25 ºC in natural sea water with corrosion products.

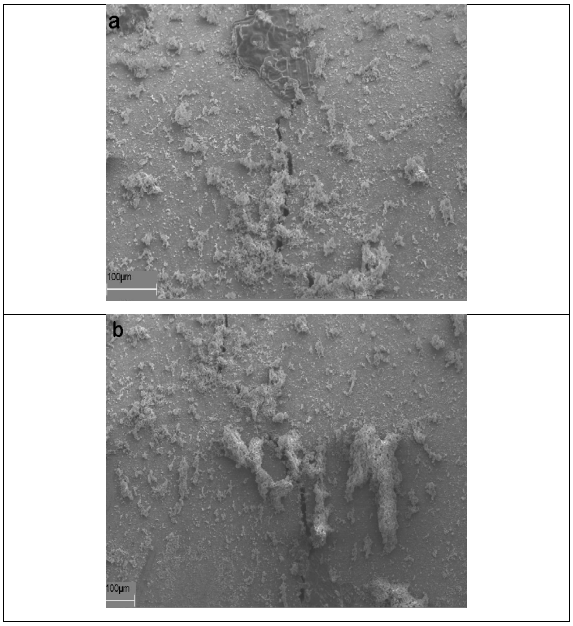

Fig. 6. Micrographs of sample B after exposure at 90 ºC in natural sea water with corrosion products.

3 Results and discussion

3.1 Physical characterization

Fig. 5 and Fig. 6 show SEM images of AISI-410 of cracked samples after exposure to natural sea water at 25 and 90 ºC respectively. These images show the presence of a significant amount of porous corrosion products at both temperatures especially at the higher temperature.

The cracks with corrosion products around them are clearly seen. From the cracks corrosion products also emerge as evidence of the oxidation process inside the cracks (Flores and Cuevas, 2017). The generation of corrosion products inside the cracks produces the growth of such cracks increasing their depth and thickness and producing a major degradation of the material.

An EDX analysis has been done to the corrosion products at both temperatures. EDX at 25 ºC shows the presence of iron, chromium and manganese (see Fig. 7.a). It is important to note that one of the peak of manganese is shared with iron and the other one with zinc and sodium. Besides taking into account that the concentration of manganese in the alloy is very low, it is concluded that this element appears in a low concentration as corrosion product. It is clear that iron and chromium are the most important elements together with oxygen, chlorine, potassium, sodium and magnesium all of them present in the seawater in high concentrations. It is possible that during the first corrosion stage iron and chromium oxides were formed being the chromium oxide the most protective one (Zakowski *et al*., 2013). Then a dissolution process was carried out forming porous oxides as shown in Fig. 5. The formation of chromium and iron chlorines is highly probably. In the case at 90 ºC some differences could be seen in the corrosion products (see Fig. 7.b): the presence of sulfur besides chlorine and silicon. The formation of silicon oxide additionally to chromium and iron oxides and the formation of chromium, iron and silicon sulfides and chlorines could have been the main corrosion products at the higher temperature (Mendoza *et al*., 2016). It could be stated that a thermal effect in the corrosion mechanism was observed producing the additional formation of silicon oxide and metallic sulphides compared to the process observed at 25 ºC (Caines *et al*., 2013).

The length and width of the cracks free of corrosion products were obtained from the SEM images presented in Fig. 8, which shows a mixed corrosion processes as localized and uniform

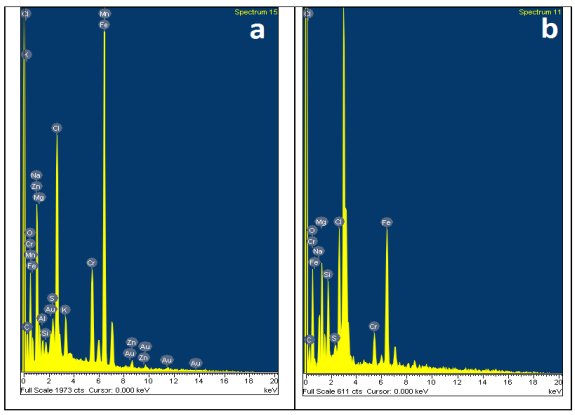

Fig. 7. EDX analysis of corroded samples at 25 ºC (a) and 90 ºC (b).

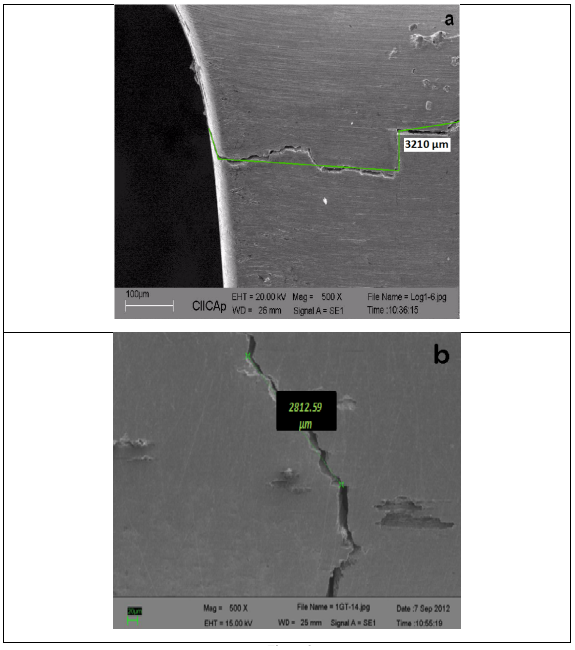

Fig. 8. Micrographs f the cracked specimens after exposing to natural sea water. a) at 25 ºC and b) at 90 ºC.

corrosion. At 90 ºC the localized corroded areas are bigger than that at the smaller temperature showing that temperature enhances localized corrosion of AISI-410. In fact at 25 ºC few small pits in a small area are presented. Being the images at the same magnification it is possible to appreciate that the width of the crack at 90 ºC is clearly longer. At the smaller temperature it seems to be that the uniform corrosion is less severe, since some evidences of ground lines are still observed.

3.2 Potentiodynamic polarization curves

Polarization curves are important to obtain some mechanistic aspects about the corrosion behavior of metallic materials. Also from polarization curves it is possible to determine some corrosion parameters such as corrosion potential (E_{corr}), corrosion current density (I_{corr}) and Tafel slopes b_a and b_c. E_{corr} and I_{corr} values indicate the corrosion activity from the point of view of thermodynamics and kinetics and not always a comparison of E_{corr} and I_{corr} are congruent (Flitt and Schweinsberg, 2005).

From polarization curves (Fig. 9) it is observed that both curves have a similar behavior. From their corrosion potential the anodic curves have an active corrosion at high scan rate, increasing the corrosion rate until to change to up to 3 mA/cm^2 at 90 ºC and 20 mA/cm^2 at 25 ºC, showing the susceptibility of AISI-410 to be corroded. Afterward the material exposed at 25 ºC presents a limit current and a decrease to 2 mA/cm^2 stating that AISI-410 was passivated. After the passivation, an activation behavior is presented until the end of both anodic curves showing a trend to get a constant current of 400 mA/cm^2 at 25 ºC and 600 mA/cm^2 at 90 ºC.

It is important to note that after the passivation, the slope of both anodic curves are different. At 90 ºC the slope is smaller than that at 25 ºC indicating the major depassivation and therefore the major susceptibility of AISI-410 to be degraded at the higher temperature. Hence the corrosion products initially more protective dissolve easily leaving the materials more exposed to be corroded, expecting that eventually the corrosion rate at the higher temperature be longer than that at the lower temperature, even though thermodynamically speaking the corrosion potential at 90 ºC resulted less negative than that at 25 ºC (Uhlig and Revie, 2008). The corrosion current density (I_{corr}) is higher at 25 ºC, nevertheless from 300 mV to the end of the experiment the corrosion current density at 90 ºC is much higher especially at 600 mV. From the physical characterization and taking into account that the crack at 90 ºC became wider, it is expected that corrosion rate be higher at the higher temperature, which would be in accord with the results from EDX analysis due to the additional presence of sulphides and the major amount of corrosion products seen in the micrographs after the exposure to the corrosive medium (See Fig. 6). The parameters from the polarization curves at both experimental temperatures are presented in Table 5.

Table 5. Parameters of AISI 410 stainless steel from potentiodynamic polarization curves.

Specimen	b_a anodic Tafel slopes (mV/dec)	b_c cathodic Tafel slopes (mV/dec)	I_{corr} (mA/cm^2)	E_{corr} (mV)
A (25 ºC)	57	53	0.088	-151.0
B (90 ºC)	81	122	0.06039	-73

In general Tafel slopes present small values especially from the anodic branch, which means that charge transfer processes control the corrosion activity and diffusion processes are relatively fast. Tafel slopes lower than 100 mV/dec are typical for activation controlled systems whereas Tafel slopes with larger values are typical for systems which are not purely activation or diffusion controlled (Skinner, 1987).

3.3 Electrochemical noise measurements

The electrochemical noise time series were used to analyze the changes in corrosion activity for AISI-410 under the experimental conditions taking into account the physical characterization of corroded samples at both temperatures (Mansfeld, 2005). Fig. 10 and 11 show the electrochemical current density and potential noise signals spectrum at different times of immersion during the five days of exposure at 25 ºC and 90 ºC respectively. The EN technique was carried out obtaining current and potential measurements each 3 h. In this work some current and potential series are presented showing the most significant patterns in order to determine the corrosion activity of AISI-410. In general the current noise exhibits high amplitude transients accompanied with random oscillations in both cases, nevertheless interesting differences are observed at each temperature. From the quantitative point of view it is possible to observe that the magnitude of the current density is in the same range in both cases, but in the case of potential the values become more active with temperature. Therefore the major corrosive activity at 90 ºC is observed and the major frequency in noise events is clearly seen, finding a great concordance between the current and the potential signals (Loto, 2012).

Also the noise pattern at both temperatures is distinct, indicating that electrochemical noise can monitor the different aspects of corrosion phenomenon. In order to describe the evolution of the noise pattern, the time series from 0 to 23 hours at each studied temperature during the indicated days will be interpreted and analyzed.

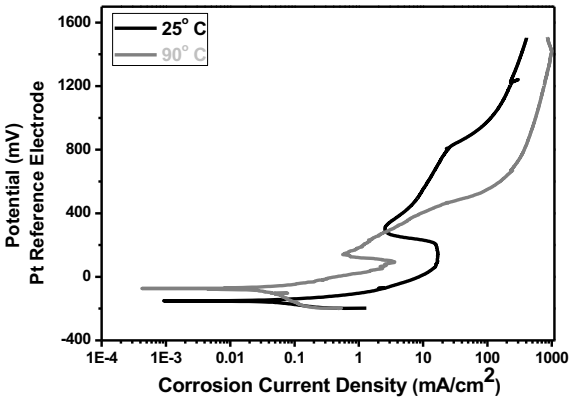

Fig. 9. Polarization curves of AISI 410 stainless steel exposed to natural sea water at 25° C and 90° C.

To deduce the corrosion mechanism of AISI-410 exposed in seawater at 25 ºC and 90 ºC, the noise pattern will be analyzed taking into account the three typical forms of electrochemical noise generated by different types of corrosion processes, which was processed without trend removal (Sánchez *et al*., 2005; Cuevas, 2005).

a) Type I (localized): Consist of transients of high intensity with a high repetition rate.

b) Type II (Mixed): It is a combination of transients of type I and oscillations of short amplitude.

c) Type III (Uniform): the pattern noise is formed by oscillations of low amplitude (white noise).

According to the behavior of the current and potential time series under the exposure at 25 ºC it can be inferred that AISI-410 suffered a kind of uniform corrosion with isolated localized events or the rupture and recovery of the passive film. In fact only at the first and fifth days some transients of low amplitude are presented. At the third day the current time series show white noise (high frequency/low amplitude). The potential noise showed a trend to become more negative in time and at the end of the experiment oscillations were presented. This behavior is typical of a system that increases its corrosion activity and

instability. The potential noise pattern presented at the third and fifth days is not very common in metallic materials with no cracks (Cuevas *et al*., 2012; Cuevas, 2012, Cuevas, 2006) since these noise pattern must reveal the presence of the corrosion inside the cracks together with the uniform and localized corrosion around the cracks. It is noted that the oscillations of potential are made over a baseline and each cycle has different frequency, which is decreasing in time at the third day and is more or less constant at the end of the exposure time. In that cases where the frequency is smaller the localized corrosion mechanism is slower and it would be state that the passivation/activation process is changing in time too slowly becoming more stable. Each potential oscillation at the third and fifth days show a slower increase in potential and a rapid decrease. The slower increase shows that the material forms a passive layer, but the rapid decrease indicates that such passive layer dissolves or breaks. This behavior is characteristic of a localized corrosion mechanism such as it was observed physically in Fig. 8. When the corrosive environment present the chlorine and sulfide species this kind of mechanism is expected (France *et al*., 1970; Strehblow, 1976; Strehblow *et al*. 1976).

The noise pattern together with the physical attack and the presence of cracks suggest that the localized corrosion is pitting/crevice, both considered to have the same mechanisms of growth and propagation (Fontana *et al*., 1978). In both types of localized corrosion exist an occluded anode or crevice whose site is free of dissolved oxygen, where metallic cations such as Fe^{2+}, Cr^{3+} or Ni^{2+} are accumulated due to the restricted mass transport to the bulk solution with anions as Cl^{1-} or S^{2-} (these species are present in seawater and also in the corrosion products of this study) which migrate into the crevice to neutralize the positive cations. The same process occur in a pit, but crevice corrosion is often thought as a special case of pitting with a ready-made initiation site. The oxidation reactions within the occluded anode liberate electrons that are consumed by the reduction reactions of some dissolved species at the surrounding cathode surfaces, which accordingly to the physical characterization are that zones around the cracks (see Fig. 8.a and 8.b) (Genesca and Ávila, 2002). The deepest sites of the existing cracks must be the anodic areas, that is why the great amount of corrosion products emerging from them. It is possible that the periodic oscillations be the result of the sum of the localized corrosion presented inside the cracks and the pitting process over the planar metallic surface, so that a very special corrosion noise pattern is revealed.

The localized process is exacerbated at 90 ºC observing some kind of different noise pattern. In this case the current and potential time series provide the same corrosion behavior, seeing medium to high intensity transients presented in a sequential way. The time series at the first hours (until 3 hours) is still of high frequency but very low intensity (white noise) indicating uniform corrosion (Loto, 2012). Even though from the first day carried out the localized corrosion process, noting that the transients at this day have lower amplitude than that presented to the following days (the current and potential scales are the same in all the graphs). At the third and fifth days most of the current time series present transients in a periodic way each 25-30 seconds, which it is interpreted as a constant and repetitive localized corrosion process inside and along the crack but also nearby the crack. Also it is probable that the lagoons of corrosion presented around the crack at this temperature be the union of many small pits since each transient represent the nucleation of a localized point of corrosion (Bertocci *et al*., 1998). Inside the cracks the corrosion process must be alike than that over the metallic surface: the formation of pits (or crevice such as it has been explained in the above paragraph for 25 ºC) together with uniform corrosion producing a great amount of corrosion products emerging from the cracks. It is important to note that the surface inside the cracks is very different since it is not grounded and therefore must present a very heterogeneous and rough surface, which represent more susceptibility to be corroded especially in a localized way. This must be the reason for which the particular type of noise pattern, where a sudden and significant increase of current (anodic) is presented followed by the decrease (cathodic) and then a recuperation over a baseline having between each transient random oscillations of very low amplitude (Cottis, 2001). The intensities of the current transients show the susceptibility of the cracks to suffer localized attack due to the heterogeneous surface inside the cracks and the presence of less resistant to corrosion elements such as iron and manganese. The negative values of current density observed at 90 ºC show the preferential dissolution of that electrode connected as the cathodic electrode hence the direction of the current has been changed (Carmel *et al*., 2000), demonstrating that AISI-410 is susceptible to be corroded in a localized way even with no cracks.

With respect to the potential time series a general behavior is observed: periodic cathodic transients

having their correspondence with the anodic current transients, representing the susceptibility of AISI-410 of corroding in a localized way. A decrease of potential to more negative or less positive values indicates the major activity in the corrosion process in localized points of the material either inside the crack or over the surface around the crack. The cathodic potential transients are presented in a repetitive way at certain time observing that at the first day is more frequently than that at the last days.

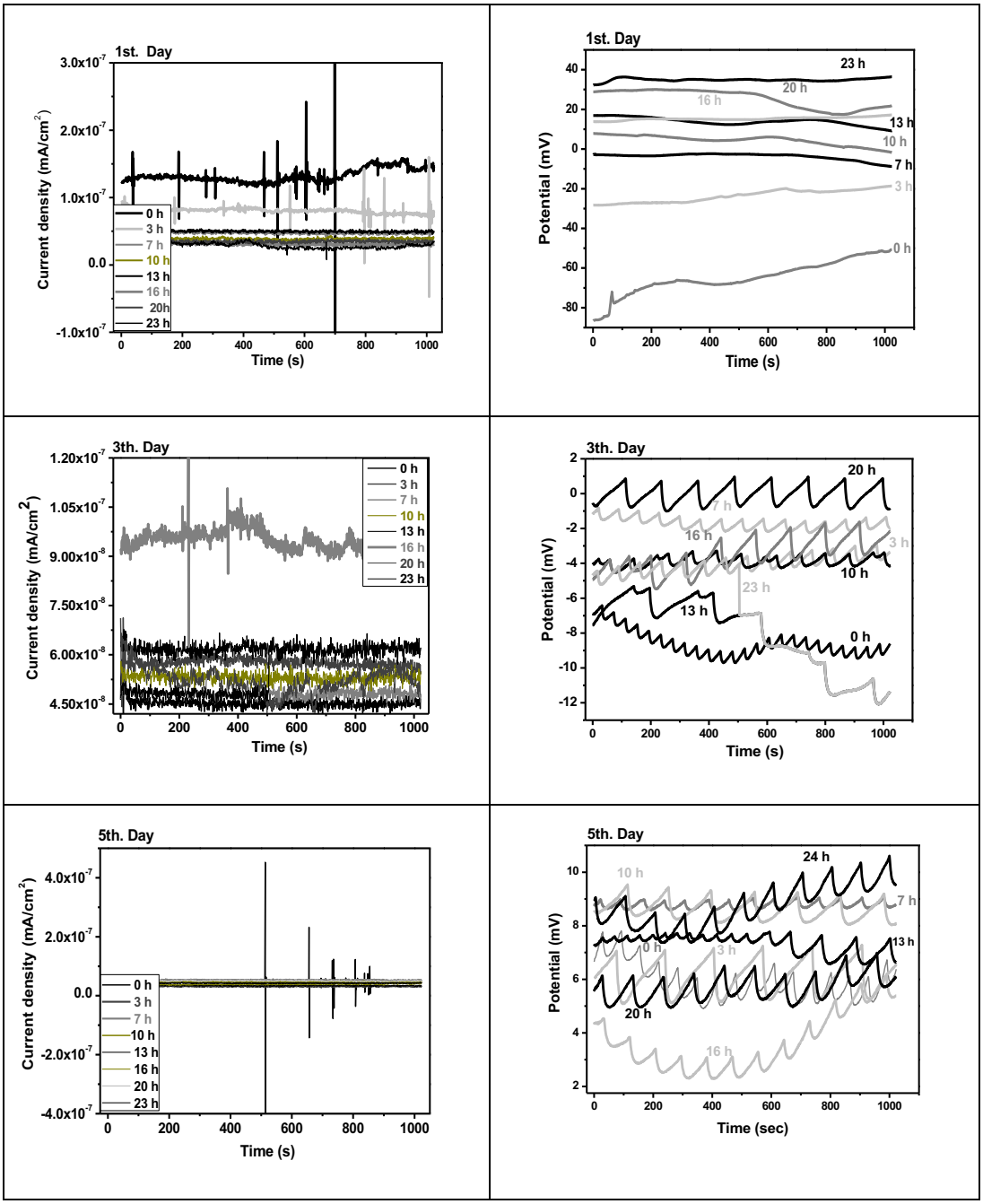

Fig. 10. Current and potential time series of AISI-410 exposed in natural sea water at 25 ºC.

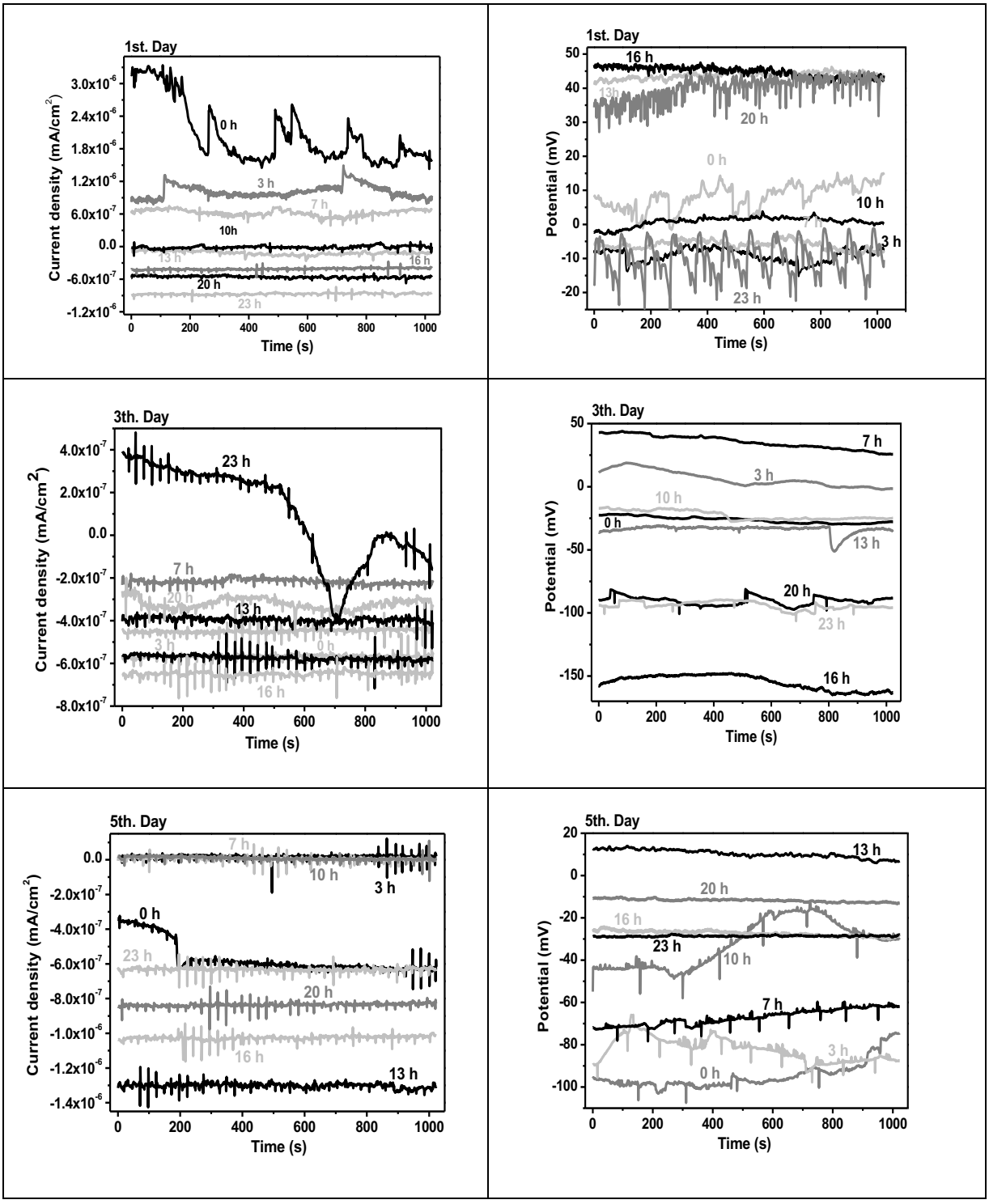

Fig. 11. Current and potential time series of AISI-410 exposed in natural sea water at 90 ºC.

At the fifth day the cathodic potential transients are presented each 100-150 seconds, so the localized process was slow at the end of the exposure time. The corrosion mechanisms presented through the current and potential electrochemical noise allows us to conclude that the presence of cracks in AISI-410 exposed in seawater especially at 90 ºC (normal condition in blades for steam turbines) can leads to stress corrosion cracking and corrosion fatigue (Cuevas *et al*., 2013), since the cracks grow due to the effect of a pitting/crevice process. Under operation conditions of blades turbines the stress is also presented, therefore in extreme localized corrosion as shown in this work a catastrophic condition could be seen in this steam systems.

In order to validate the behavior of the electrochemical noise signals with respect to the corrosion process the localization index (LI) was calculated as the ratio between the current noise standard deviation σ_i over the root-mean-square current value Irms (Cottis *et al*., 1999; Mansfeld *et al*., 1998; Alawadhi *et al*., 1999, Scully, 1995) which is presented as indicator of localized corrosion activity. The analysis took into account the different ranges of LI values, which lie between 0.0 and 1.0. For larger current fluctuations compared to the mean current, LI will have values close to 1.0; while for small current fluctuations LI will be close to 0.0 (Fontana *et al*. 1978, France *et al*. 1970). The values of the localization index are shown in Fig. 12. LI values were calculated from each time series records obtained from the electrochemical noise measurements. LI values are mainly positioned in the mixed corrosion zones at both temperatures observing just few points in the localized zone at 25 ºC and some more at 90 ºC.

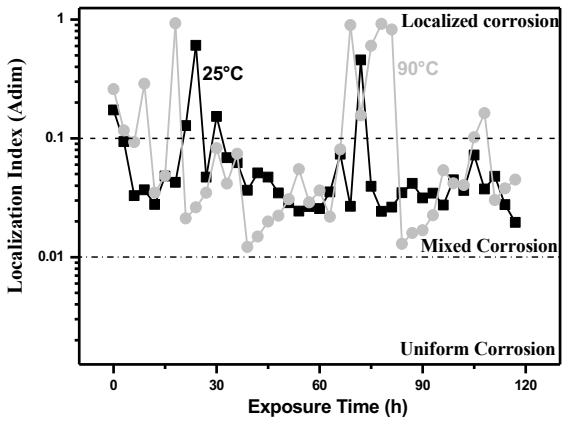

Fig. 12. Localization index of AISI-410 exposed in natural sea water at 25 and 90 ºC.

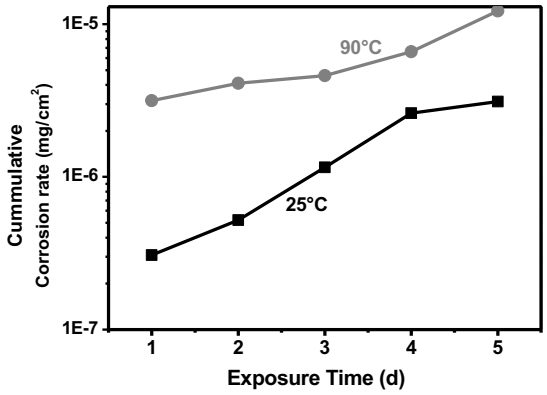

Fig. 13. Cumulative corrosion rate of AISI-410 exposed in natural sea water at 25 and 90 ºC.

These results are due to the fact that at 25 ºC there were few transients at low intensity while at 90 ºC several significant transients could be seen as an indicative that the localized process was more evident at the higher temperature. From EN results it concludes that the localization index is considered as an indicator of the prevailing corrosion mechanism (Mansfeld, 1999).

Fig. 13 shows the experimental cumulative corrosion rate (C_{corr}) in time obtained from the electrochemical noise data for AISI-410 stainless steel exposed to seawater at the two test temperatures. In order to calculate the mass loss in time, the noise resistance Rn was evaluated as the ratio of the potential noise standard deviation over the current noise standard deviation (Cottis *et al*., 1999; Mansfeld *et al*., 1998; Alawadhi *et al*., 1999, Scully, 1995; Mansfeld *et al*., 1997). Then Rn data were used in the Stern-Geary equation to obtain the corrosion current density I_{corr} (mA/cm^2). Subsequently the Faraday's Law (Mansfeld *et al*., 1998; Scully, 1995; Mansfeld *et al*., 1997; ASTM G102-89, 2015) was utilized to obtain the mass loss as described elsewhere (Cuevas *et al*. 2006; Cuevas and Porcayo 2006). It was necessary to obtain the Tafel slopes to calculate the Tafel constant B present in the Stern-Geary equation. Tafel slopes were determined from the experimental polarization curves at the test temperatures (see Table 5). The behavior of the corrosion kinetics at 25 ºC showed that the corrosion rate had a tendency to increase in time, observing that at the last day had a tendency to get a constant value. The corrosion rate at 25 ºC had the smallest values compared to that at 90 ºC. This result is also in accord with the visual characterization obtained from SEM analysis

since the crack has minor growth and the localized corrosion seemed to be smaller than that at 90 ºC. The trend to get constant values at the end of the experiment at 25 ºC is an indication that AISI-410 at this temperature could be protected such as it was also shown through the potentiodynamic polarization curve where passivation was observed tending to get a current limit at the highest potential. The corrosion kinetic at 90 ºC tended to increase in time along the experimental time, observing a major slope at the last day as an indicative that the corrosion is more active due to the great localized corrosion and the major growth of the crack, which was monitored congruently with the electrochemical noise technique noting that the noise pattern at 90 ºC presented a typical behavior of a very severe localized corroded system. The presence of sulfur as corrosion product may lead the formation of metallic sulphides in combination with the porous oxide layer, which interferes with the passivation process.

Conclusions

Through the application of potentiodynamic polarization curves and the electrochemical noise techniques it was possible to carry out a study of pitting/crevice corrosion in AISI-410 stainless steel immersed in seawater at 25 ºC and 90 ºC. The current and potential time series showed a noise pattern typical of a mixed corrosion process with a severe localized process, showing the repetitive presence of transients of significant intensities especially at the highest test temperature. The presence of high intensity transients at high frequency was a response of a localized process mainly presented inside and around the cracks producing an important growth of the cracks. The pitting corrosion was also seen outside the crack in minor extent together with uniform corrosion. According to the behavior of the noise pattern the cracks and its heterogeneous surface in AISI-410 were the preponderant reason to encourage localized pitting and crevice corrosion.

Results from physical characterization of corroded samples and polarization curves were in agreement with the electrochemical current and potential time series, where the corrosion phenomenon of AISI-410 exposed to seawater was observed thermally active. The localization index parameter for this corrosive system can be considered as a complement to conclude that current and potential noise signals represent in a great extent the corrosion mechanism carried out when AISI-410 with cracks is immersed in seawater at 25 and 90 ºC. From the results of this study it appears that AISI-410 used in blades turbines could suffer a catastrophic damage due stress and pitting/crevice corrosion under such operation conditions.

Nomenclature

b_a	Anodic Tafel slope, mV/dec
b_c	Cathodic Tafle slope, mV/dec
C_{corr}	Cumulative corrosión rate, mg cm^{-2}
E_{corr}	Corrosion Potential, mV
f	Load frequency, cpm
I_{corr}	Corrosion current density, mA cm^{-2}
LI	Localization index, adim
L	Stress load, MPa
N	Cycles
T	Time, s, h, d
W	Weight, %

Greek Simbols

σ_i	Current noise standard deviation, adim
Δ_k	Stress intensity at the crack tip, MPa

References

Alawadhi A.A., Cottis R.A. (1999). Electrochemical noise signature analysis using power and cross-spectral densities. *CORROSION/1999, (NACE-International) 207*, 1-24.

Andrade C., Muñoz A., and Torres Acosta A. (2010). Correlation between crack width of concrete cover and corrosion of reinforcing elements exposed to a natural environment contaminated by chlorides. *Concrete and Cement, Researcher and development, [In: Spanish] 1-2*, 30-41.

ASTM E647 88A (2011). Standard Test Method for Measurement of Fatigue Crack Growth Rates.

ASTM G1-03 (2017). Standard Practice for Preparing, Cleaning, and Evaluating Corrosion Test Specimens.

ASTM G31-72 (2004). Standard Practice for Laboratory Immersion Corrosion Testing of Metals.

ASTM G102-89 (2015). Standard Practice for Calculation of Corrosion Rates and Related Information from Electrochemical Measurements.

ASTM G199-09 (2014) Standard Guide for Electrochemical Noise Measurement.

Baboian R. (2002). *NACE Corrosion Engineer's Reference Book*, Third edition.

Bertocci U., J. Frydman J., GabrieIIi, C., Huet F., Keddam M. (1998). Analysis of electrochemical noise by power spectral density applied to corrosion studies: Maximum entropy method or fast Fourier transform. *Journal of the Electrochemical Society 145*, 2780-2786.

Carmel B., Rudd Amy L. (2000). Activation of pure Al in an indium-containing electrolyte – An electrochemical noise and impedance study. *Corrosion Science 42*, 1023-1039.

Caines S., Khan F, John Shirokoff J. (2013). Analysis of pitting corrosion on steel under insulation in marine environments. *Journal of Loss Prevention in the Process Industries 26*, 1466-1483.

Cottis, R. A., Turgoose, S. (1999). *Electrochemical Impedance and Noise*, (B. Syrett ed.), NACE Corrosion Testing Made Easy, Houston.

Cottis, R. A. (2001). Interpretation of electrochemical noise data. *Corrosion 57*, 265-285.

Cuevas Arteaga C. (2005). Proceedings of the European Corrosion Congress EFC, Event No. 273, Lisbon Portugal. *Portuguese Materials Society (Ed), Paper B-13*.

Cuevas-Arteaga C. (2006). Cinéticas de corrosión del acero inoxidable SS-304 expuesto en una solución acuosa de bromuro de litio a bajas temperaturas. *Revista Mexicana de Ingeniería Química 5*, 27-45.

Cuevas-Arteaga C., Porcayo-Calderón J. (2006). Electrochemical noise analysis in the frequency domain and determination of corrosion rates for SS-304 stainless steel. *Materials Science and Engineering A 435-436*, 439-446.

Cuevas-Arteaga C. (2008). Corrosion study of HK-40m alloy exposed to molten sulfate/vanadate mixtures using the electrochemical noise technique. *Corrosion Science 50*, 650-663.

Cuevas Arteaga C., Porcayo Calderón J., Campos Sedano C. F., Rodríguez J. A. (2012). Comparison of Corrosion Resistance of Carbon Steel and Some Stainless Steels Exposed to LiBr-H_2O Solution at low Temperatures. *International Journal of Electrochemical Science 7*, 445-470.

Cuevas-Arteaga C. (2012). Corrosion Evaluation of AISI-309 exposed to 50 mol% Na_2SO_4-50 mol% V_2O_5 at high temperature applying electrochemical techniques and the weight loss method. *International Journal of Electrochemical Science 7-1*, 12283-12300.

Cuevas-Arteaga C., Rodríguez J.A., Clemente C.M., Segura J. A., Urquiza U. (2013). Estimation of useful life in turbines blades with cracks in corrosive environment. *Engineering Failure Analysis 35*, 576-589.

Genesca J., Ávila J. (2002). *Más allá de la Herrumbre*. Vol. I. Editorial Fondo de cultura económica.

Estupiñán-López F.H., Almeraya-Calderón F., Bautista Margulis R.G., Baltazar Zamora M.A., Martínez-Villafañe A., Uruchurtu J., Gaona-Tiburcio C. (2011). Transient analysis of electrochemical noise for 316 and duplex 2205 stainless steels under pitting corrosion. *Int. J. Electrochem. Sci. 6*, 1785-1796.

Flitt H. J., Schweinsberg D.P. (2005). Evaluation of corrosion rate from polarization curves not exhibiting a Tafel region. *Corrosion Science 47*, 3034-3052.

Flores García N. S., Cuevas-Arteaga C. (2017). High temperature corrosion investigation of the Inconel-600 in molten sulfate/vanadate mixtures using electrochemical techniques. *International Journal of Electrochemical Science 12*, 9882-9895.

Fontana M. G. and Greene N. D. (1978). *Corrosion Engineering*, 2nd. Edn. Chapters 9 and 10, McGraw-Hill, New York.

France W. D., and Greene N. D. (1970). Comparison of chemically and electrolytically induced pitting corrosion. *Corrosion 26*, 1-4.

Kubiak J., González J.G., Sierra F.Z., García J.C., Nebradt J., and Salinas V.M. (2005). Failure of last-stage turbine blades in a geothermal power plant. *Journal of Failure Analysis and Prevention 5*, 26-32.

Loto C. A. (2012). Electrochemical noise measurement technique in corrosion research. *Int. J. Electrochem. Sci. 7*, 9248-9270.

Mendoza M.D, Cuevas Arteaga C. (2016). Determination of the corrosion resistance of SS-304 in synthetic seawater at two temperatures using electrochemical noise and polarization curves. *Int. J. Electrochem. Sci. 11*, 8683 -8696.

Mansfeld F., Han L.T., Lee C.C, Chen C., Zhang G. and Xiao H. (1997). Analysis of electrochemical impedance and noise data for polymer coated metals. *Corrosion Science 39-2*, 255-279.

Mansfeld F., Lee C.C. and Zhang G. (1998). Comparison of electrochemical impedance and noise data in the frequency domain. *Electrochimica Acta 43-3/4*, 435-438.

Mansfeld F., Sun Z. (1999). Technical note: Localization index obtained from electrochemical noise analysis. *Corrosion 55*, 915-918.

Mansfeld F. (2005). *The Electrochemical Noise Technique-Applications in Corrosion Research*, 18th International Conference on Noise and Fluctuations-ICNF, Edited by T. Gonzalez, J. Mateos, D. Pardo.

Sanchez-Amaya J.M, Cottis R.A, Bontana F.J. (2005). Shot noise and statistical parameters for the estimation of corrosion mechanisms. *Corrosion Science 47-12*, 3280-3299.

Sánchez Amaya J. E., Bethencourt M., González Rovira M., Botana Y. F.J. (2009). Measurement of electrochemical noise for the study of corrosion processes of metallic alloys. *Revista de Metallurgia 45-2*, 143-156.

Scully John R. (1995). *Electrochemical, Corrosion Tests and Standards: Application and Interpretation*, (Robert Baboian ed.), ASTM Manual Series: MNL 20, chapter 7, 75-90.

Skinner, K. (1987). Influence of experimental inaccuracies on corrosion rates and Tafel slopes determined from electrochemical measurements in different overpotential ranges. *British Corrosion Journal 22-3*, 172-175.

Strehblow, H. (1976). Nucleation and repassivation of corrosion pits for pitting on iron and nickel. *Werkstoffe und Korrosion 27-11*, 792-799.

Strehblow H. H. and Ives M. B. (1976). On the electrochemical conditions within small pits. *Corrosion Science 16-5*, 317-318.

Tristancho J.L, Báez S, Peña M., Vásquez J. (2004). Application of electrochemical noise technique for evaluation of hot corrosion by molten salts. *Journal of Latin America and the Caribbean, Spain and Portugal [In: Spanish] 71-144*. 82-92.

Turnbull A., Zhou S. (2011). Comparative evaluation of environment induced cracking of conventional and advanced steam turbine blade steels. Part 2: Corrosion fatigue. *Corrosion Science 53*, 503-512.

Uhlig H.H. and Revie R.W. (2008). *Corrosion and Corrosion Control*, Wiley and Sons, New Jersey, USA.

Zakowski K, Szocinski M, Narozny M. (2013). Study of the formation of calcareous deposits on cathodically protected steel in Baltic sea water. *Anti-Corrosion Methods and Materials 60-2*, 95-99.